



PCCP

**Vibrational predissociation versus intramolecular vibrational energy redistribution (IVR) in rare gas...dihalogen complexes: IVR identified in Ar...I<sub>2</sub>(B,v') using velocity-map imaging**

Journal:	<i>Physical Chemistry Chemical Physics</i>
Manuscript ID	CP-PER-10-2021-004727.R1
Article Type:	Perspective
Date Submitted by the Author:	15-Nov-2021
Complete List of Authors:	Makarem, Camille; Washington University in St Louis, Chemistry Wei, Jie; Washington University in St Louis, Chemistry Loomis, Richard; Washington University in St Louis, Chemistry Darr, Joshua; University of Nebraska Omaha, Chemistry

SCHOLARONE™  
Manuscripts

## PERSPECTIVE

## Vibrational predissociation versus intramolecular vibrational energy redistribution (IVR) in rare gas...dihalogen complexes: IVR identified in Ar...I<sub>2</sub>(B,ν') using velocity-map imaging

Received 00th January 20xx,  
Accepted 00th January 20xx

DOI: 10.1039/x0xx00000x

Camille Makarem,<sup>a,b</sup> Jie Wei,<sup>a</sup> Richard A. Loomis<sup>\*a</sup> and Joshua P. Darr<sup>\*c</sup>

The competition between multiple pathways sampled during the energetic relaxation of excited molecules can be difficult to experimentally decipher. The rare gas...dihalogen van der Waals complexes have remained key systems for exploring the competition between relaxation pathways, such as intramolecular vibrational energy redistribution (IVR) and vibrational predissociation (VP). As these mechanisms can yield the same products, the relaxation pathways traversed are often deduced from the excitation spectra or product-state distributions. In addition to a brief perspective on IVR and VP in rare gas...dihalogen complexes, we present new results obtained using time-of-flight velocity-map imaging (VMI) on T-shaped Ar...I<sub>2</sub>(B,ν',n'=0) complexes that illustrate how contributions from these two pathways can be separated. The angular anisotropies of the ion images collected for the I<sub>2</sub>(B,ν<ν') fragments indicate the products for certain Ar...I<sub>2</sub>(B,ν',n'=0) levels are weighted along the direction perpendicular to the laser-polarization axis. These distributions are consistent with prompt dissociation of the T-shaped excited-state complexes, likely via direct VP. The distributions measured for other Ar...I<sub>2</sub>(B,ν',n'=0) levels are preferentially along the laser-polarization axis. These initially prepared levels must undergo IVR with nearly resonant Ar...I<sub>2</sub>(B,ν<ν',n>0) intermolecular vibrational levels that sample linear Ar-I-I orientations during dissociation.

### 1 Introduction

The stabilization of weakly-bound van der Waals complexes and the interrogation of the dynamics incurred following photoexcitation offer valuable opportunities for investigating energy transfer dynamics that often can be extended to more complicated systems and environments. When the complexes are simple enough and their spectroscopies are well characterized, specific “bright” intermolecular vibrational levels can be prepared in low-lying electronic states. The resultant dynamics, which often include dissociation, represent half-collision events originating from a limited range of impact parameters dictated by the properties of that initially prepared state.

The three-atom, weakly-bound rare gas...dihalogen complexes, including those with heteronuclear dihalogens, XY, or homonuclear dihalogens, X<sub>2</sub>, have proven valuable for gaining insights into intermolecular interactions, energy-transfer processes, and dynamics within and between small molecules with limited degrees of freedom.<sup>1-10</sup> These complexes are ideal for study in part because of their structural simplicity and the strong optical properties they exhibit in the B(<sup>3</sup>Π<sub>0u</sub><sup>+</sup>) – X(<sup>1</sup>Σ<sub>0g</sub><sup>+</sup>)

visible spectral region of the dihalogens. Most of the energy-transfer and dynamics experiments have been performed following excitation of the complexes to the lowest-energy levels, n'=0, bound within the Rg + XY(B,ν') or Rg + X<sub>2</sub>(B,ν') intermolecular potential energy surfaces (PESs) with varying amounts of dihalogen vibrational excitation, ν'. The geometries of the complexes in these intermolecular levels are rigidly T-shaped, or nearly T-shaped for the Rg...XY complexes, with the Rg atom localized within a minimum of the PES at an orientation that is orthogonal to the dihalogen bond between the two halogen atoms.<sup>8-13</sup> Despite the general similarities of the different Rg + XY(B,ν') and Rg + X<sub>2</sub>(B,ν') PESs, the strengths of the interactions, the vibrational frequencies of the dihalogens, and the densities of intermolecular states associated with them give rise to contrasting relaxation mechanisms and dissociation dynamics.

The prominent relaxation pathways that effectively compete with fluorescence of the initially prepared intermolecular vibrational levels of the Rg...XY(B,ν',n'=0) and Rg...X<sub>2</sub>(B,ν',n'=0) complexes are vibrational predissociation (VP), intramolecular vibrational energy redistribution (IVR), and electronic predissociation (EP).<sup>9,10</sup> The EP pathway results in separate Rg + X + Y or Rg + X + X atomic products, and it can effectively compete with radiative relaxation or fluorescence signals. The contributions in the excited-state dynamics associated with EP can be monitored by probing the yields and dynamics of the halogen-atom products.<sup>14</sup> Ultimately, both VP and IVR result in Rg and XY(B,ν) or X<sub>2</sub>(B,ν) fragments, and the excited dihalogen molecular products then relax via fluorescence

<sup>a</sup> Department of Chemistry, Washington University in St. Louis, One Brookings Drive, CB 1134, Saint Louis, MO 63130, USA

<sup>b</sup> Present Address: OptoKnowledge Systems, Inc., Torrance, CA 90502, USA

<sup>c</sup> Department of Chemistry, University of Nebraska at Omaha, 6001 Dodge St, DSC 337, Omaha, NE 68182, USA

\* loomis@wustl.edu; jdarr@unomaha.edu

Electronic Supplementary Information (ESI) available: [details of any supplementary information available should be included here]. See DOI: 10.1039/x0xx00000x

that can be detected in laser-induced fluorescence, fluorescence excitation, or dispersed fluorescence measurements. As both VP and IVR can result in the formation of the same product channels, deciphering the contributions of these two channels can be difficult, and an array of experimental and theoretical work has focused on characterizing these channels for the  $n' = 0$  T-shaped level of the  $\text{Rg}\cdots\text{XY}(\text{B},v')$  and  $\text{Rg}\cdots\text{X}_2(\text{B},v')$  complexes. Herein, we provide a brief overview of VP and IVR in  $\text{Rg}\cdots\text{X}_2(\text{B},v')$  complexes and focus on new results obtained for the  $\text{Ar}\cdots\text{I}_2(\text{B},v',n'=0)$  complex. Specifically, data acquired in ion time-of-flight velocity map imaging (VMI) experiments indicate that complexes prepared in T-shaped  $\text{Ar}\cdots\text{I}_2(\text{B},v',n'=0)$  levels can yield distinctly different  $\text{I}_2(\text{B},v<v')$  product angular distributions. These differences are associated with the nature of intermediate  $\text{Ar}\cdots\text{I}_2(\text{B},v<v',n>0)$  levels sampled during IVR.

These results on the dissociation dynamics of the three-atom,  $\text{Ar}\cdots\text{I}_2$  system offer promise for deciphering the competing pathways sampled during the prompt dissociation dynamics of even larger systems.

## 2 Overview

### 2.1 Direct Vibrational Predissociation

Dissociation of weakly-bound, homonuclear  $\text{Rg}\cdots\text{X}_2(\text{B},v',n'=0)$  van der Waals complexes has been observed to proceed via different mechanisms and along parallel channels. An energy schematic illustrating the PESs and levels summarizing the direct VP mechanism is shown in **Figs. 1(a)** and **(b)**. Direct VP involves the coupling of the initially prepared, metastable  $n' = 0$  intermolecular vibrational level bound within the  $\text{Rg} + \text{X}_2(\text{B},v')$

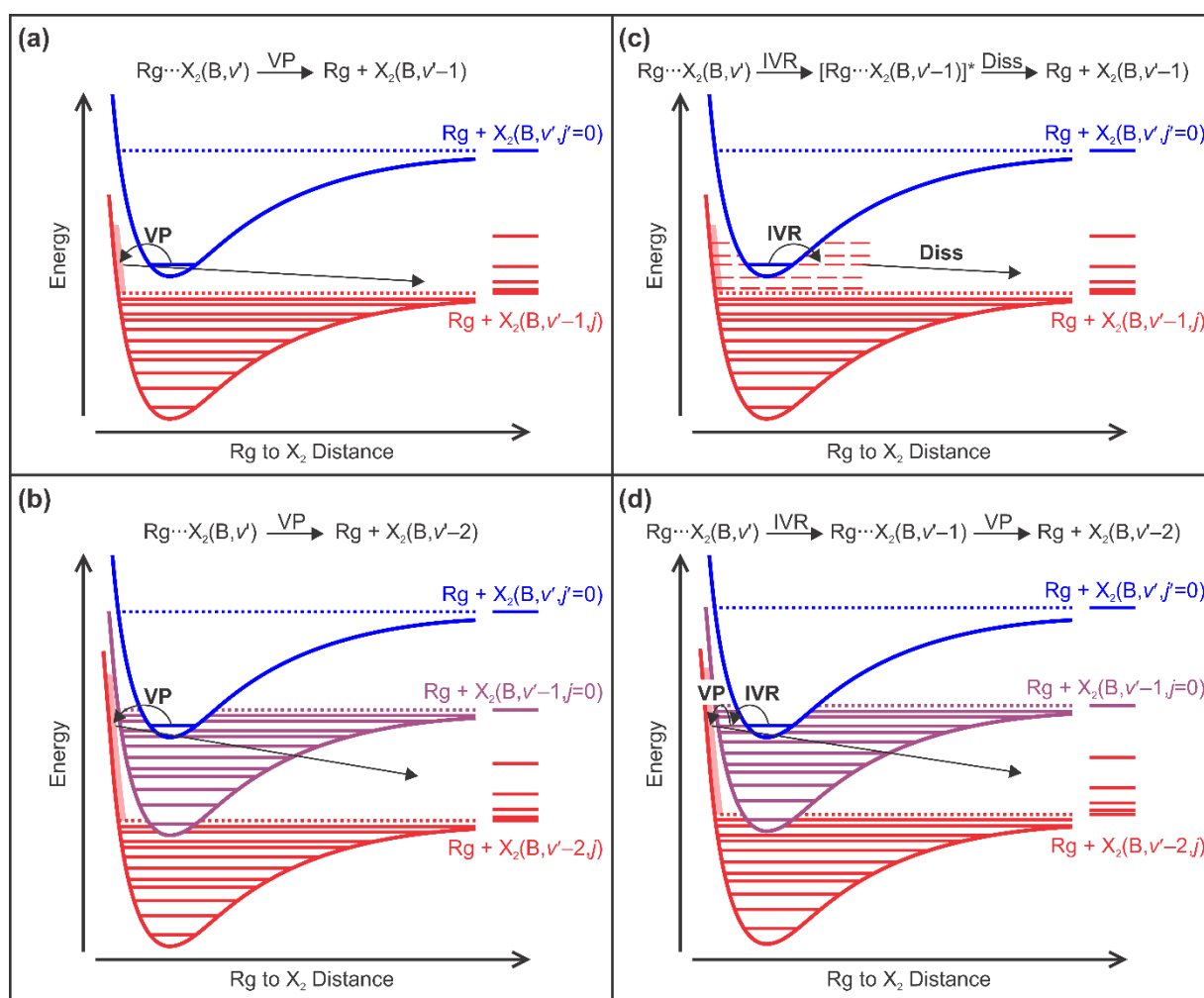


**Fig. 1** Vibrational predissociation (VP) and intramolecular vibrational relaxation (IVR) relaxation mechanisms of electronically-excited rare gas...dihalogen complexes,  $\text{Rg}\cdots\text{X}_2(\text{B},v,n')$ . (a) VP occurs by the coupling of  $\text{X}_2$  vibrational excitation to the  $\text{Rg}\cdots\text{X}_2$  intermolecular vibration coordinate. If the  $\text{X}_2(\text{B},v)$  vibrational spacing is larger than the  $\text{Rg} + \text{X}_2(\text{B},v)$  binding energy, this occurs by preferential coupling to the continuum of states and direct dissociation to the  $\text{Rg} + \text{X}_2(\text{B},v-1,j)$  products. (b) If the  $\text{X}_2(\text{B},v)$  vibrational spacing is smaller than the  $\text{Rg} + \text{X}_2(\text{B},v)$  binding energy, VP occurs by preferential coupling to the continuum of states and direct dissociation to the highest-energy product channel, in this case the  $\text{Rg} + \text{X}_2(\text{B},v-2,j)$  products. (c) When the  $\text{X}_2(\text{B},v)$  vibrational spacing is larger than the  $\text{Rg} + \text{X}_2(\text{B},v)$  binding energy, IVR may occur via the coupling of the initially prepared  $\text{Rg}\cdots\text{X}_2(\text{B},v,n'=0)$  level to a metastable  $\text{Rg}\cdots\text{X}_2(\text{B},v-1,n')$  level (dashed lines) that dissociates into  $\text{Rg} + \text{X}_2(\text{B},v-1,j)$  products. (d) When the  $\text{X}_2(\text{B},v)$  vibrational spacing is smaller than the  $\text{Rg} + \text{X}_2(\text{B},v)$  binding energy and the potentials are nested within each other, IVR may occur via the coupling of the initially prepared  $\text{Rg}\cdots\text{X}_2(\text{B},v,n'=0)$  level to an isoenergetic level with intermolecular vibrational excitation bound within a lower-lying potential,  $\text{Rg}\cdots\text{X}_2(\text{B},v-1,n')$ . This  $\text{Rg}\cdots\text{X}_2(\text{B},v-1,n')$  level may also undergo additional IVR, but VP will ultimately result in the formation of  $\text{X}_2(\text{B},v,j)$  products with  $v \leq v-2$ .

PES to the continuum of states energetically lying above the  $Rg + X_2(B, v < v')$  dissociation limit.<sup>1,7,10,11,15-33</sup> The complex dissociates with the excess energy above the dissociation limit partitioned into translational excitation of the  $Rg$  product and both translational and rotational excitation of the  $X_2(B, v, j)$  products. The asymptotes of the  $X_2(B, v)$  product rotational states,  $j$ , are illustrated to the right in **Fig. 1(a)**. Direct VP for the  $\Delta v = -1$  channel is typical for the  $He \cdots X_2(B, v', n'=0)$  complexes as their binding energy is often substantially less than the  $X_2$  vibrational spacing, especially for low  $v'$ .

In the VP of the T-shaped  $Rg \cdots X_2(B, v', n'=0)$  complexes, the dominant  $X_2(B, v)$  product is usually associated with the highest energetically accessible vibrational quantum number  $v$ . As described above, for  $He \cdots X_2$  complexes, this usually corresponds to the  $\Delta v = -1$  channel. However, oftentimes for  $Rg \cdots X_2$  complexes containing a heavier and more polarizable  $Rg$  atom, such as  $Ne$  or  $Ar$ , the conservation of energy precludes VP through the  $\Delta v = -1$  channel, and VP must occur via the loss of two or more  $X_2$  vibrational quanta, as illustrated in **Fig. 1(b)**. In this case, the binding energies of the  $Rg \cdots X_2(B, v)$  complexes are large enough that the PESs are nested inside one another. Thus, the  $n' = 0$  metastable intermolecular vibrational level bound within the  $Rg + X_2(B, v')$  PES is lower in energy than the asymptote of the  $Rg + X_2(B, v'-1)$  PES. Consequently, the first accessible product channel is the  $\Delta v = -2$  channel associated with the  $Rg + X_2(B, v'-2)$  PES. VP then occurs as complexes in the initially prepared  $Rg \cdots X_2(B, v', n'=0)$  level couple directly to the continuum of states lying above the asymptote associated with the  $Rg + X_2(B, v'-2)$  PES, generating products with  $Rg$  translational energy and  $X_2(B, v'-2, j)$  translational and rotational energy.

The examples presented in **Fig. 1** are simplistic scenarios illustrating the formation of the highest-energy VP product channels. The VP mechanism can also form products associated with lower energy asymptotes, such as the  $\Delta v = -3$  or  $-4$  channels, as their continua of dissociative states can also be accessed from the initially prepared level. Ultimately, the conservation of energy, Franck-Condon factors of the dihalogen and intermolecular levels, and momentum conservation all contribute to the yields for the different channels.

## 2.2 Dissociation Involving IVR

In addition to dissociation of weakly-bound  $Rg \cdots X_2(B, v', n'=0)$  complexes via a direct VP mechanism, numerous studies have concluded that dissociation can also occur through an IVR mechanism.<sup>7,9,26,33-49</sup> As with direct VP, dissociation via IVR can proceed either through the loss of a single vibrational quantum of the  $X_2$  stretch, the  $\Delta v = -1$  channel, or through the loss of two or more vibrational quanta of the  $X_2$  stretch. In the case of the former, the PESs are not nested within one another, while in the latter, they most often are. The IVR dissociation mechanisms proceeding through these two scenarios are illustrated in **Figs. 1(c)** and **(d)**, respectively.

**Fig. 1(c)** illustrates an IVR dissociation mechanism that occurs predominantly through the  $\Delta v = -1$  channel. In this pathway, the initially-prepared  $Rg \cdots X_2(B, v', n'=0)$  complex couples to a state representing a resonance above the asymptote

associated with the  $Rg + X_2(B, v'-1)$  PES, red dashed lines. The difference between this dissociation mechanism and that shown in **Fig. 1(a)** is that this resonance level likely has internal bending or hindered-rotor character with the  $Rg$  atom delocalized about the  $X_2$  moiety and is stabilized by a centrifugal barrier. The coupling of a rigidly T-shaped  $n' = 0$  level in the  $Rg + X_2(B, v')$  PES to highly-excited  $Rg \cdots X_2(B, v < v', n > 0)$  levels represents an energy redistribution involving both the  $X_2(B, v)$  molecular and the intermolecular van der Waals coordinates and, consequently, an IVR process. Free rotor-type resonances, such as these, have been spectroscopically identified by Darr, et al.<sup>50</sup> After coupling to a “dark” resonance level, the complex dissociates forming  $Rg + X_2(B, v, j)$  products with translational and rotational energy.

IVR can also occur when forming  $Rg + X_2(B, v)$  products with the dihalogen losing more than a single quantum of vibrational excitation, e.g. the  $\Delta v = -2$  channel. This IVR-mediated, VP mechanism is shown in **Fig. 1(d)**. In this case, the intermolecular PESs associated with multiple  $X_2(B, v)$  vibrational states are usually nested in each other. Complexes in the initially-prepared  $Rg \cdots X_2(B, v', n'=0)$  level couple with an isoenergetic level or levels with significant intermolecular vibrational excitation,  $n > 0$ , that are bound within a  $Rg + X_2(B, v < v')$  PES. Again, since this mechanism involves a change in  $v$  and  $n$ , it is referred to as an IVR mechanism. The accessed  $Rg \cdots X_2(B, v < v', n > 0)$  level is also metastable, and it can undergo additional IVR or undergo direct VP, coupling to the continuum of states above the asymptote of the  $Rg + X_2(B, v'-2)$  PES for this schematic, forming  $Rg + X_2(B, v'-2, j)$  products with translational energy. As for direct VP, this last step can also access the continua above the lower-energy asymptotes, and the  $\Delta v = -3, -4$ , or other  $I_2(B, v)$  channels may be formed.

## 2.3 IVR Regimes

The efficiency for IVR from the bright  $Rg \cdots X_2(B, v', n'=0)$  level to dark  $Rg \cdots X_2(B, v < v', n > 0)$  levels depends on the density of the dark states, the coupling strengths between the bright and dark states, and the energetic overlap of these states.<sup>41,48,51,52</sup> The coupling strength gives rise to a homogeneous broadening of each resonance,  $\Gamma$ , that can blend together the dark states, which are energetically separated by  $\Delta$ . In the sparse IVR regime, either  $\Delta$  is large (a small density of dark states) or  $\Gamma$  is small, and  $\Gamma < \Delta$ . Here, the  $n' = 0$  bright state comes into and out of resonance with the dark states with increasing  $v'$ .<sup>39,41,47</sup> Since the efficiency for VP typically increases smoothly with  $v'$ , IVR in the sparse regime would result in varying or oscillatory lifetimes with  $v'$ .<sup>9,47,53</sup> Furthermore, the specific nature of the dark states accessed would likely yield rotational-state distributions of the  $X_2(B, v)$  products that are characteristic of that dark state.<sup>46</sup>

In contrast, if the coupling strength for IVR is large or if the density of states is large then  $\Gamma > \Delta$ , and there is a near-continuum of coupling states and a small dependence of the efficiency for IVR on  $v'$ .<sup>41</sup> In this statistical regime, the lifetimes of the excited-state complexes decrease monotonically with  $v'$ . Furthermore, the nature of the different dark states is lost as they energetically overlap each other due to large  $\Gamma$  or small  $\Delta$ . As a result, the rotational-state distributions of the  $X_2(B, v)$  products

should be statistical, and they are not expected to change significantly with  $v'$ .<sup>46</sup>

#### 2.4 Evidence for IVR-Mediated Dissociation

Contributions from IVR-mediated dissociation in weakly-bound  $\text{Rg}\cdots\text{X}_2(\text{B},v',n'=0)$  van der Waals complexes have been inferred from results obtained using different experimental techniques. The fluorescence quantum yields were measured for excitation of the  $\text{He}\cdots\text{Br}_2$  and  $\text{Ne}\cdots\text{Br}_2$  complexes to the T-shaped,  $n' = 0$  levels with varying  $\text{Br}_2(\text{B},v')$  vibrational excitation.<sup>54</sup> The variations in the quantum yields for those complexes were attributed to the irregular contributions from IVR to the excited-state dynamics. Frequency-resolved laser spectroscopy was used to measure linewidths of the vibronic features associated with transitions to the different  $\text{Rg}\cdots\text{X}_2(\text{B},v',n'=0)$  levels in the  $\text{X}_2\text{B}-\text{X}$ ,  $v'-0$  region. For several systems,  $\text{He}\cdots\text{I}_2$ ,<sup>1,16,17,55</sup>  $\text{Ne}\cdots\text{I}_2$ ,<sup>1</sup>  $\text{He}\cdots\text{Br}_2$ ,<sup>30,56,57</sup>  $\text{Ne}\cdots\text{Br}_2$ ,<sup>22</sup> and  $\text{Ar}\cdots\text{Cl}_2$ ,<sup>26,58</sup> the linewidths of the features oscillate with  $v'$ , and thus the excited-state lifetimes of the complexes were observed to correspondingly vary when accessing states where the  $\text{Rg} + \text{X}_2(\text{B},v'-1)$  product channel was energetically closed due to the anharmonicity of the  $\text{X}_2(\text{B},v)$  potential. The dissociation mechanism for these systems was associated with IVR as shown in **Fig. 1(d)** with the bright  $\text{Rg}\cdots\text{X}_2(\text{B},v',n'=0)$  levels coming in and out of resonance with dark  $\text{Rg}\cdots\text{X}_2(\text{B},v<v',n)$  levels in the sparse IVR regime.

Additional evidence for IVR-mediated dissociation in weakly-bound  $\text{Rg}\cdots\text{X}_2$  van der Waals complexes has been observed in the rotational-state distributions of the  $\text{X}_2(\text{B},v',j)$  products.<sup>46</sup> Based upon a direct VP mechanism, most rotational-state distributions are expected to follow a half-collision model of dissociation. However, some  $\text{Rg}\cdots\text{X}_2$  van der Waals complexes were found to have highly erratic or bimodal  $\text{X}_2(\text{B},v',j)$  product rotational-state distributions.<sup>46</sup> These non-smoothly varying distributions were interpreted as representing coupling through an intermediate dark or “doorway” state as illustrated in **Figs. 1(c)** and **(d)**.

Perhaps the most definitive evidence for IVR in the dissociation of  $\text{Rg}\cdots\text{X}_2(\text{B},v',n'=0)$  levels was reported by Cabrera, et al.<sup>59</sup> They examined both the decay of signals associated with complexes in the initially prepared  $\text{Ne}\cdots\text{Br}_2(\text{B},v',n'=0)$  levels and the rise of signals associated with the  $\text{Br}_2(\text{B},v<v')$  products using time-resolved, pump-probe spectroscopy. They determined the timescales for the disappearance of the  $\text{Ne}\cdots\text{Br}_2(\text{B},v',n'=0)$  complexes was notably faster than those for the appearance of the  $\text{Br}_2(\text{B},v<v')$  products. These authors convincingly argued that intermediate  $\text{Ne}\cdots\text{Br}_2(\text{B},v<v',n>0)$  “doorway” states must be accessed. They invoke a picture similar to **Fig. 1(c)** for low and mid-range  $v'$ , and a mechanism more like that depicted in **Fig. 1(d)** for high  $v'$ .

#### 2.5 IVR in $\text{Ar}\cdots\text{I}_2(\text{B},v')$

IVR has been extensively studied in the  $\text{Ar}\cdots\text{I}_2(\text{B},v',n'=0)$  system, likely more than any of the other  $\text{Rg}\cdots\text{X}_2(\text{B},v',n'=0)$  complexes. Complexes with heavier, more polarizable rare gas atoms tend to have larger binding energies,  $D_0'$ , and the  $\text{Rg} + \text{X}_2(\text{B},v')$  PESs become nested within each other when  $D_0'$  is larger than the energetic spacing between the  $\text{X}_2(\text{B},v)$  and

$\text{X}_2(\text{B},v'-1)$  levels. For example,  $\text{Ar}\cdots\text{I}_2$  complexes in the B-state have binding energies of  $\sim 227\text{ cm}^{-1}$ , and three quanta of iodine vibrational energy is necessary for dissociation of complexes prepared in the lowest-energy, T-shaped,  $n' = 0$  level bound within the  $\text{Ar} + \text{I}_2(\text{B},v'\leq 29)$  PESs.<sup>2,60</sup> Due to the anharmonicity of the vibrational motion in the B electronic state, the  $\Delta v = -3$  product channel closes at  $v' > 29$  for the T-shaped  $\text{Ar}\cdots\text{I}_2(\text{B},v',n'=0)$  complexes, and at least four quanta of  $\text{I}_2$  vibrational energy are required for dissociation ( $\Delta v \leq -4$ ).

Due to the large binding energy of the  $\text{Ar}\cdots\text{I}_2(\text{B},v')$  complexes, the nesting of their PESs within each other, and the resultant high density of dark states, the  $\text{Ar}\cdots\text{I}_2(\text{B},v',n'=0)$  complexes have been proposed to dissociate via IVR. Furthermore, the smooth, monotonic decrease of the complex lifetimes with increasing  $v'$  and the lack of pronounced structure in the rotational-state distributions of the  $\text{I}_2(\text{B},v<v')$  products suggest that IVR occurs in the statistical regime.<sup>7,34,44-46</sup> These experimental results, however, contradict calculations that indicate there are only a few  $\text{Ar}\cdots\text{I}_2$  states that lie close in energy to the initially prepared level and that can couple and enable IVR to occur.<sup>39,42,43</sup> More recent spectroscopy experiments identified highly-excited  $\text{Ar}\cdots\text{I}_2(\text{B},v',n'>0)$  intermolecular vibrational levels, and it was determined the density of states is more accurately described as being in the sparse regime for IVR.<sup>61</sup>

In the efforts reported here, time-of-flight velocity-map imaging (VMI) was used to characterize the angular distribution of  $\text{I}_2(\text{B},v<v')$  fragments following dissociation of  $\text{Ar}\cdots\text{I}_2(\text{B},v',n'=0)$  levels, where  $v' = 16-39$ . The angular distributions of the  $\text{I}_2(\text{B},v<v')$  fragments provide direct experimental evidence of IVR occurring from  $\text{Ar}\cdots\text{I}_2(\text{B},v',n'=0)$  levels. Furthermore, this information along with the spectral assignments of the  $\text{Ar}\cdots\text{I}_2$  transitions in the  $\text{I}_2\text{B}-\text{X}$ ,  $v'-0$  region<sup>61</sup> and the intermolecular vibrational level wavefunctions calculated by Roncero, et al.,<sup>62</sup> allow us to propose intermolecular vibrational levels that may be involved in the IVR. More generally, these results demonstrate VMI as a promising and direct means to observe energy redistribution in photo-excited van der Waals complexes where competing pathways leading to the same product channels, such as VP and IVR, are present.

### 3 Experimental

Details of the apparatus have been previously described.<sup>60</sup> The ground-state  $\text{Ar}\cdots\text{I}_2(\text{X},v''=0)$  complexes were stabilized in a pulsed supersonic expansion by passing a 5% Ar in He carrier gas mixture (8500-11000 Torr) over a vessel containing room-temperature iodine crystals. A pulsed valve (800  $\mu\text{m}$  diameter opening) operating at 15 Hz was used to expand the sample into the source chamber, which was kept at an average pressure of  $7.5 \times 10^{-6}$  Torr during operation of the valve. The laser pulses were generated by two dye lasers, each pumped by the 355 nm output of a separate pulsed Nd:YAG laser.

The pulsed supersonic expansion was intersected orthogonally by the laser-pulse axis  $\sim 60$  mm downstream from the nozzle. LIF spectra were recorded to identify transitions of the T-shaped  $\text{Ar}\cdots\text{I}_2(\text{X},v''=0)$  complex in the different  $\text{I}_2\text{B}-\text{X}$ ,  $v'-0$  spectral regions. To collect these spectra, the excitation laser

was scanned throughout various  $I_2$  B–X,  $v' = 0$  spectral regions, and the resultant fluorescence was imaged onto a photomultiplier tube (PMT) using an optical telescope assembly. A 600 nm long wave pass filter was used to preferentially collect fluorescence from the  $I_2(B)$  electronic state. The supersonic expansion was passed through a 2 mm skimmer mounted 110 mm from the pulsed valve. The skimmer was used to collimate the expansion before entering the ionization region of the chamber and to provide differential pumping between the source chamber and the ionization region of the apparatus. The ionization region was evacuated with a turbomolecular pump to a pressure of  $<4 \times 10^{-8}$  Torr during an experiment.

In the VMI experiments, the wavenumber of the excitation laser,  $E_1$ , was fixed on a transition of the ground-state T-shaped  $Ar \cdots I_2(X, v'' = 0)$  complex to the rigidly T-shaped,  $n' = 0$  lowest-energy intermolecular vibrational level bound within the  $Ar + I_2(B, v')$  PES.<sup>61</sup> The second laser,  $E_2$ , was used to ionize the resulting  $I_2(B, v)$  products via (1+1) resonantly-enhanced multiphoton ionization (REMPI) through vibrational levels in the  $E(3\Pi_{0g^+})$  ion-pair state.<sup>63</sup> The probe laser pulses, focused by a 100 cm focal length lens, were delayed 50 ns from the excitation laser pulses. Both lasers were linearly polarized and oriented parallel to the ion detector face (vertical on the camera). The  $I_2^+$  cations were then accelerated through a time-of-flight (TOF) tube, with a length of 1.57 m and a pressure of  $\sim 1 \times 10^{-8}$  Torr, using an ion optics set-up following the design of Eppink and Parker,<sup>64</sup> with the repeller electrode placed 52 mm downstream from the skimmer. The cations were directed onto a chevron-type multi-channel plate (MCP) detector with a P20 phosphor screen. The MCP was time-gated for the arrival of  $I_2^+$  cations. Because of the low kinetic energy of the  $I_2(B, v)$  products and the corresponding  $I_2^+$  cations along the flight tube region, repulsion between the ions often lead to elongation of the images. In order to avoid this, the laser pulse energy fluences were lowered to reduce the ion density. The excitation and probe laser pulse energies were kept between 0.5–1.0 mJ and 0.2–0.4 mJ, respectively. The excitation and ionization laser beams were  $\sim 2$  mm and  $\sim 2.2$  mm in diameter yielding typical laser fluences of  $\sim 6$  and  $\sim 2$  mJ  $cm^{-2}$ , respectively. The number of ions detected per laser shot was 3–7. The ion images were acquired using a charge-coupled device (CCD) camera and accumulated over at least 100,000 laser pulses for each image.

Ion-yield spectra were recorded in order to gain information about the  $I_2(B, v, j)$  product rotational-state distributions and the dissociation mechanisms for forming the different states. These distributions were collected by fixing the wavenumber of the excitation laser,  $E_1$ , on a particular T-shaped  $Ar \cdots I_2$  transition in the  $I_2$  B–X,  $v' = 0$  region, as with the VMI experiments, and scanning the probe laser,  $E_2$ , near an  $I_2$  (1+1) REMPI transition. Instead of using a CCD camera to image the ions on the phosphor screen, a PMT was used to collect the total intensity from the phosphor screen as each ion was detected. The integrated intensity of the ion signals recorded as a function of the probe transition wavenumber,  $E_2$ , provided each ion-yield spectrum.

## 4 Results and Discussion

LIF spectra were recorded in the same manner as reported previously to identify the transitions of the T-shaped complexes that were used in the dissociation dynamics experiments.<sup>60</sup> Fig. 2 includes an LIF spectrum collected by scanning  $E_1$  through the  $I_2$  B–X, 38–0 spectral region. The T-shaped  $Ar \cdots I_2$  B–X, 38–0 transition is observed near 19213  $cm^{-1}$  along with the broad continuum fluorescence signals associated with bound-free transitions of the linear  $Ar \cdots I_2(X, v'' = 0)$  conformer. Spectroscopic assignments of the transitions of both the T-shaped and linear conformers were identified previously using action spectroscopy, as they are not easily identified in LIF spectra.<sup>61</sup> The six lowest-energy features in each spectral region are localized in the T-shaped region, and 11 features to higher energies spanning up to the dissociation limit are associated with transitions of the linear conformer to delocalized intermolecular vibrational levels. Although the densities of states are sufficiently high that a T-shaped level in an  $Ar + I_2(B, v')$  PES may be isoenergetic with a high-lying level in a lower  $Ar + I_2(B, v < v')$  PES, the different ground-state binding energies of the ground-state conformers result in no accidental degeneracies of the T-shaped transitions with linear transitions in the spectral regions explored in the work presented herein. The arrows in Fig. 2 indicate the transitions used to excite the T-shaped complex and the continuum in the VMI experiments, which were chosen to avoid discrete linear transitions.

A few of the VMI images obtained for the  $I_2(B, v \leq v' - 3)$  products collected after excitation in different  $I_2$  B–X,  $v' = 0$  spectral regions are included in Fig. 3. The images in the first row, (a), (e), and (i), were obtained with  $E_1$  fixed on transitions to the indicated T-shaped  $Ar \cdots I_2(B, v')$  levels and  $E_2$  fixed on the rotational bandhead, and thus low rotational states, of the (1+1) REMPI transitions using the indicated product level in the  $I_2$  E–B,  $v^\dagger - v$  spectral region. When exciting the T-shaped transitions, however, bound-free transitions of the linear  $Ar \cdots I_2(X, v'' = 0)$  conformer are also induced since the T-shaped features are superimposed on the linear continuum fluorescence signals. In order to characterize the dynamics of only the  $I_2(B, v)$  products formed from VP of the T-shaped complexes, it was necessary to remove the contributions from the linear bound-free excitation. To correct for this, images included in the second row of Fig. 3, (b), (f), and (j), were collected with  $E_1$  fixed just 2.5

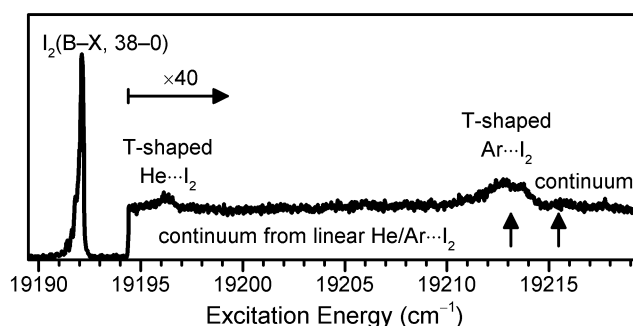
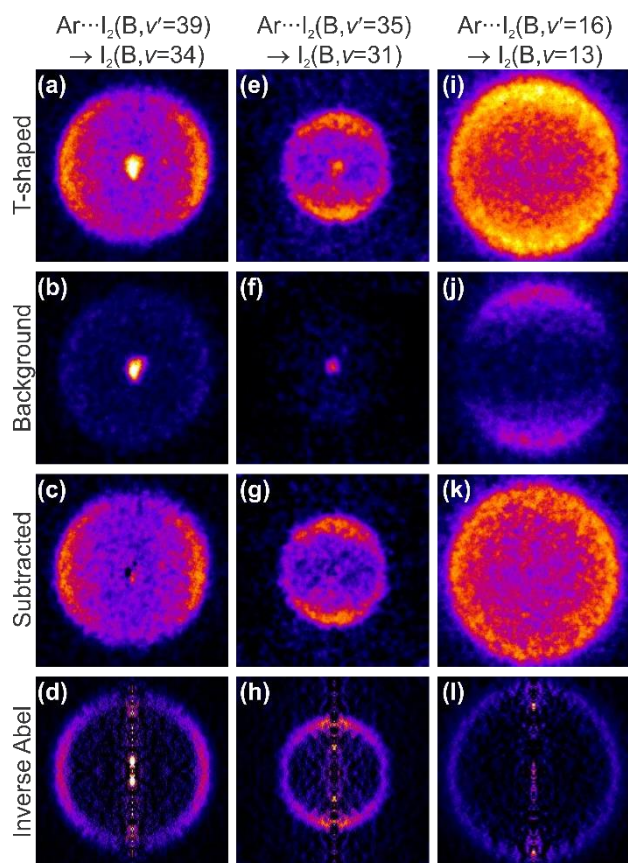


Fig. 2 LIF spectrum recorded in the  $I_2$  B–X, 38–0 spectral region. Features from transitions of the ground-state T-shaped complexes are labelled, as is the continuum fluorescence signal due to bound-free transitions of the ground-state linear complexes. The vertical arrows indicate the transition wavenumbers used to excite the T-shaped complex and continuum.



**Fig. 3** Velocity-map images of  $I_2(B, v)$  fragments following dissociation of the  $n' = 0$ , T-shaped  $Ar \cdots I_2(B, v'=39)$  (first column),  $Ar \cdots I_2(B, v'=35)$  (second column), and  $Ar \cdots I_2(B, v'=16)$  (third column) complexes. The images in each column were obtained with the (1+1) REMPI laser fixed on the  $I_2$  E-B, 71-34, 71-31, and 54-13 transitions, respectively. The first row includes the raw images collected with the excitation laser fixed on the peak of the T-shaped bands. The second row includes the images of the background ions collected with the excitation laser fixed 2.5  $cm^{-1}$  higher in energy than the T-shaped bands. The third row includes the background-subtracted images of the  $I_2(B, v)$  products formed by the dissociation of the T-shaped  $Ar \cdots I_2(B, v')$  complexes, and the inverse Abel transform of these images yield the two-dimensional slices of the product momentum distributions, included in the fourth row. The intensity scales in the first three rows remain constant, but the intensity scales for the transformed images are adjusted for clarity.

$cm^{-1}$  higher than the T-shaped transitions so that the kinetic energy distribution for the background, continuum signals are nearly the same as those of the T-shaped transition.  $E_2$  was fixed on the same REMPI transitions of the  $I_2$  E-B,  $v^+ - v$  rotational bandheads. The resulting images included only the fragments that were produced from the bound-free transitions of the linear complex. In order to remove these contributions from the first image, the images in the second row were subtracted from the images in the first row, and the continuum-corrected images are included in the third row, panels (c), (g), and (k).

Each velocity-map image is a projection of the 3-dimensional velocity distribution of the products onto the detector surface. An inverse Abel transform was performed on each of these images using the BASEX program.<sup>65</sup> The fourth row in **Fig. 3**, panels (d), (h), and (l), includes the inverse Abel transformation of the background-subtracted image of the  $I_2(B, v)$  products. Particular attention was paid to characterizing the

angular distributions or  $I_2^+$  product image anisotropies. The photofragment angular distribution is expressed by<sup>66</sup>

$$I(\theta) = \frac{1}{4\pi} (1 + \beta \cdot P_2(\cos\theta)), \quad (1)$$

where  $\theta$  is defined as the angle between the laser polarization axis (vertical) and the momentum vector of the fragments.  $P_2(\cos\theta)$  is the second Legendre polynomial, and  $\beta$  is the anisotropy parameter. It follows that the limiting values of  $\beta$  are +2 for fragments dissociating parallel to the polarization axis and  $\beta = -1$  for fragments dissociating perpendicular to the polarization axis.<sup>66</sup> **Table 1** lists a summary of the anisotropy of the  $I_2(B, v')$  fragment data collected.

The use of polarized excitation light defines the initial alignment of the molecules upon excitation. The transition moment of the  $Ar \cdots I_2$  molecule is along the I-I bond axis, and the  $I_2$   $B(^3\Pi_{0u}^-) - X(^1\Sigma_{0g}^+)$  transition is a parallel transition. When exciting transitions of the T-shaped complexes to the lowest levels in the  $Ar + I_2(B, v')$  PESs, which also have rigid T-shaped geometries, those complexes whose I-I axis is oriented along the laser polarization axis will preferentially be excited, as illustrated in **Fig. 4**. If the T-shaped  $Ar \cdots I_2(B, v')$  complexes dissociate promptly via VP, the trajectory of  $I_2$  fragments will be perpendicular to the laser polarization axis and will have a  $\sin^2\theta$  fragment angular distribution, as indicated in **Fig. 4**(a). This gives an anisotropy parameter approaching  $\beta = -1$ .

The first column in **Fig. 3** includes ion image data obtained with promotion of the complexes to the T-shaped  $Ar \cdots I_2(B, v'=39, n'=0)$  level,  $E_1 = 19267.11$   $cm^{-1}$ , and detection of the rotationally cold  $I_2(B, v=34)$  products with  $E_2 = 28633.7$   $cm^{-1}$ . The  $I_2(B, v=34)$  fragments have a noticeable anisotropy with  $\beta = -0.58(1)$ , which is consistent with dissociation from a T-shaped geometry. Products with  $\beta < 0$  could be produced via direct VP from the initial state or IVR through a dark intermolecular level localized within the T-shaped well region of any of the  $Ar + I_2(B, v=35-38)$  PESs. The product images

**Table 1** Anisotropy parameters and proposed intermediate levels involved in the IVR of the initially prepared  $Ar \cdots I_2(B, v')$  level when forming the  $Ar + I_2(B, v)$  fragments.

$v'$	$v$	$\Delta v$	$\beta$	Proposed IVR Coupling
16	13	-3	-0.08(2)	--
21	18	-3	+0.22(2)	$\Delta v = -2$
23	20	-3	+0.18(1)	$\Delta v = -2$
26	23	-3	+0.30(1)	$\Delta v = -2$
27	23	-4	-0.03(5)	$\Delta v = -1 / \Delta v = -2$
29	26	-3	-0.03(2)	--
	25	-4	-0.39(1)	$\Delta v = -1$
	24	-5	-0.39(1)	$\Delta v = -1$
	23	-6	-0.16(3)	$\Delta v = -1$
33	28	-5	+0.03(2)	--
35	31	-4	+0.67(2)	$\Delta v = -3$
	30	-5	+0.64(2)	
36	32	-4	+0.67(2)	$\Delta v = -3$
	31	-5	+0.66(3)	
	30	-6	+0.79(6)	
37	32	-5	+0.07(1)	$\Delta v = -1 / \Delta v = -3$
38	34	-4	-0.25(2)	$\Delta v = -1$
	33	-5	-0.67(1)	
	32	-6	-0.80(2)	
	31	-7	-0.80(2)	
39	34	-5	-0.58(1)	$\Delta v = -1$
	33	-6	-0.33(1)	
	32	-7	-0.02(2)	--

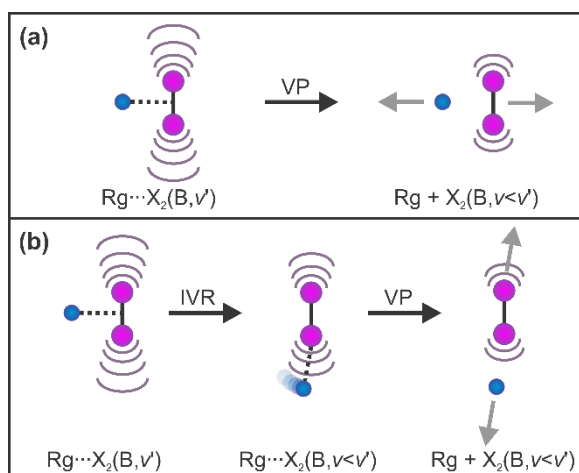


**Fig. 4** Schematic depictions of how dissociation could result in  $X_2(B, v)$  products preferentially along the horizontal,  $\theta = 90^\circ$ , or vertical,  $\theta = 0^\circ$  and  $180^\circ$ , directions. In these experiments, the vertical polarization of the excitation laser,  $E_1$ , preferentially excites complexes with the I–I bond axis also along the vertical direction. **(a)** Prompt VP of the initially prepared T-shaped  $Rg \cdots X_2(B, v')$  level would form products along  $\theta = 90^\circ$ . **(b)** Dissociation that occurs via IVR and then VP could result in  $X_2(B, v)$  products along any angular coordinate dictated by the intermediate level accessed.

collected for the T-shaped  $Ar \cdots I_2(B, v'=29)$  and  $Ar \cdots I_2(B, v'=38)$  levels also had similar angular distributions.

The VMI data collected when exciting a few T-shaped  $Ar \cdots I_2(B, v', n'=0)$  levels revealed  $I_2$  fragment images with positive anisotropy parameters, as indicated in **Table 1**. The images collected when exciting the T-shaped  $Ar \cdots I_2(B, v'=35, n'=0)$  level with  $E_1 = 19043.1 \text{ cm}^{-1}$  and probing  $\Delta v = -4$ ,  $I_2(B, v=31)$  fragments with  $E_2$  fixed on the rotational bandhead of the  $I_2$  E–B, 71–31 transition at  $28828.6 \text{ cm}^{-1}$  is an example of these distributions, middle column of **Fig. 3**. Analysis of the continuum-corrected and inverse-Abel transformed image, **Fig. 3(h)** determined  $\beta = +0.67(2)$ . Thus, despite the  $\cos^2(\theta)$  distribution of the I–I bonds within the rigid T-shaped  $Ar \cdots I_2(B, v'=35)$  complexes and a corresponding  $\sin^2(\theta)$  distribution of the Ar– $I_2$  intermolecular bond axis relative to the vertical, laser polarization axis, the  $Ar + I_2(B, v=31)$  fragments are formed with velocity components preferentially along the vertical polarization axis. This cannot occur from the initially prepared intermolecular vibrational level. Instead, the initially prepared level must couple with another intermolecular vibrational level that has the Ar– $I_2$  intermolecular bond axis preferentially along the polarization axis. We conclude the complexes initially prepared in the  $Ar \cdots I_2(B, v'=35, n'=0)$  intermolecular vibrational level undergo IVR into  $Ar \cdots I_2(B, v, n > 0)$  levels with intermolecular vibrational excitation that are bound in lower lying  $Ar + I_2(B, v=32-34)$  PESs. These levels accessed via IVR are likely high-lying bending or hindered internal-rotor levels where the Ar is somewhat delocalized about the I–I bond axes, sampling the linear geometry. A cartoon of this proposed IVR mechanism is included in **Fig. 4(b)**.

The  $I_2(B, v=13)$  products imaged after preparation of the T-shaped  $Ar \cdots I_2(B, v'=16, n'=0)$  level with  $E_1 = 17527 \text{ cm}^{-1}$  and  $E_2 = 29051.7 \text{ cm}^{-1}$  have a nearly isotropic angular distribution,  $\beta = -0.08(2)$ . For  $Ar \cdots I_2(B, v', n'=0)$  levels with low  $v'$ , an

isotropic distribution may be the result of dissociation of an excited-state complex that is long lived in comparison to the rotational period of the complex. Complexes prepared in the  $Ar \cdots I_2(B, v'=16, n'=0)$  level were estimated to have a lifetime of  $\sim 150 \text{ ps}$ , which is on the order of the rotational period of the complex.<sup>29,39</sup>

The numerous intermolecular vibrational levels bound within the  $Ar + I_2(B, v')$  PESs, which were recently identified in action spectroscopy experiments, provide insights into those levels that may be accessed in the IVR mechanism.<sup>61</sup> These levels are illustrated schematically in **Fig. 5(a)**. The blue levels, labelled a through f, are localized in the T-shaped well, and the higher-energy red levels, labelled g through q, are delocalized in

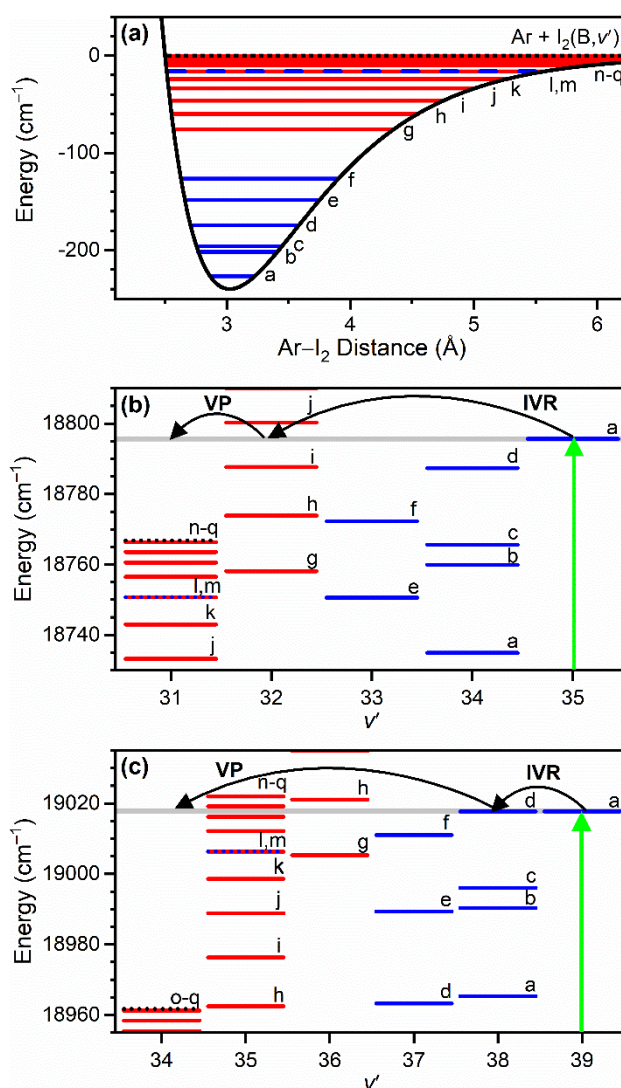


**Fig. 5 (a)** Identified intermolecular vibrational levels in the  $Ar + I_2(B, v')$  PES.<sup>61</sup> Panels **(b)** and **(c)** include the intermolecular levels bound within the  $v = 31-35$  and  $v = 34-39$  manifolds that the T-shaped  $Ar \cdots I_2(B, v', n'=0)$  complexes with  $v' = 35$  and  $v' = 39$  may couple with via IVR. The green vertical arrows indicate excitation to the initial  $Ar \cdots I_2(B, v', n'=0)$  level with an energy indicated by the gray, horizontal line. Red lines represent intermolecular vibrational levels that are delocalized in the angular coordinate, sampling the linear geometry. Blue lines represent levels that are localized in the T-shaped region of the intermolecular PES. Only those levels with wave functions having even symmetry about the  $C_{2v}$  axis are included. The black curved arrows indicate the proposed level involved in IVR.

the angular coordinate and sample the linear geometry. The blue dashed line, labelled *l*, is an intermolecular level in the  $\text{Ar} + \text{I}_2(\text{B}, \nu')$  PES that is accessed by both the ground-state linear and T-shaped  $\text{Ar} \cdots \text{I}_2(\text{X}, \nu''=0)$  conformers. Not all of the intermolecular levels could be identified in the action spectroscopy experiments since transitions of the T-shaped  $\text{Ar} \cdots \text{I}_2(\text{X}, \nu''=0)$  ground-state conformer can only access excited-state levels that have symmetric intermolecular wave functions about the  $\text{C}_{2v}$  axis.<sup>61</sup> The spectroscopy experiments specifically identified those levels bound within the  $\text{Ar} + \text{I}_2(\text{B}, \nu')$  PESs with  $\nu' = 20$ –23, but the energies of the levels relative to the dissociation limit for each PES do not change significantly with  $\nu'$ . We approximate the energies of the intermolecular vibrational levels bound within all of the  $\text{Ar} + \text{I}_2(\text{B}, \nu')$  PESs involved in the dynamics experiments investigated here using those of the  $\nu' = 20$ –23 PESs. Due to the anharmonicity of the  $\text{I}_2(\text{B})$  potential, those intermolecular vibrational levels that may be in energetic resonance with each of the prepared T-shaped  $\text{Ar} \cdots \text{I}_2(\text{B}, \nu')$  levels will depend on  $\nu'$ .

A schematic of those intermolecular vibrational levels that may participate in the IVR of the initially prepared  $\text{Ar} \cdots \text{I}_2(\text{B}, \nu'=35, n'=0)$  level is presented in **Fig. 5(b)**. The T-shaped  $\text{Ar} \cdots \text{I}_2(\text{B}, \nu'=35)$  complex could couple with excited intermolecular levels bound within the  $\text{Ar} + \text{I}_2(\text{B}, \nu=32$ –34) PESs, since the  $\Delta\nu = -4$ ,  $\text{Ar} + \text{I}_2(\text{B}, \nu=31)$  channel is the first energetically accessible dissociation channel. Based on the energy-level schematic, the *d* level within the  $\text{Ar} + \text{I}_2(\text{B}, \nu=34)$  PES lies close in energy to the initially prepared  $\text{Ar} \cdots \text{I}_2(\text{B}, \nu'=35, n'=0)$  level. This level, however, remains within the T-shaped well, and it likely does not access the linear orientation indicated by the image anisotropy. Instead, level *i* bound within the  $\text{Ar} + \text{I}_2(\text{B}, \nu=32)$  PES represents a high-lying, bending or hindered-rotor level that samples the linear geometry. After coupling with level *i*, the next step in the dissociation mechanism would be VP to the continuum of states above the  $\text{Ar} + \text{I}_2(\text{B}, \nu'=31)$  product channel, yielding the observed positive anisotropy parameter.

Those levels that produce fragments with positive anisotropy parameters provide direct evidence of IVR, whether it occurs from IVR to a metastable level, as indicated in **Fig. 1(c)**, or from IVR followed by VP as indicated in **Fig. 1(d)**. This is in agreement with the quantum dynamics calculations performed by Roncero and Gray,<sup>39</sup> which determined that the density of states in the  $\text{Ar} + \text{I}_2(\text{B}, \nu')$  PESs is such that VP is always mediated by IVR and direct VP of the complex is unlikely.

Some of the ion images collected when preparing T-shaped  $\text{Ar} \cdots \text{I}_2(\text{B}, \nu', n'=0)$  levels reveal  $\text{I}_2$  fragments images with negative anisotropy parameters, as indicated in **Table 1**. The ion images collected when exciting the  $\text{Ar} \cdots \text{I}_2(\text{B}, \nu'=39, n'=0)$  level with  $E_1 = 19627.1 \text{ cm}^{-1}$  and probing  $\Delta\nu = -5$  fragments in the  $\text{Ar} + \text{I}_2(\text{B}, \nu=34)$  product with  $E_2 = 28633.7 \text{ cm}^{-1}$  channel are examples of these distributions, and these are included in the first column of **Fig. 3**. The continuum-corrected image in Panel (c) and its inverse Abel transform, Panel (d), give a negative anisotropy parameter of  $-0.58(1)$ , which indicates prompt dissociation perpendicular to the polarization axis.

While negative anisotropy parameters are indicative of dissociation from a T-shaped geometry, they do not exclude the possibility of IVR. **Fig. 5(c)** includes a schematic of those intermolecular vibrational levels that may be involved in the IVR of  $\text{Ar} \cdots \text{I}_2(\text{B}, \nu'=39, n'=0)$ . The  $\Delta\nu = -5$  channel corresponding to  $\text{Ar} + \text{I}_2(\text{B}, \nu=34)$  products is the first energetically available dissociation channel. As a result, the prepared T-shaped  $\text{Ar} \cdots \text{I}_2(\text{B}, \nu'=39, n'=0)$  level could couple with excited intermolecular levels bound within the  $\text{Ar} + \text{I}_2(\text{B}, \nu=35$ –38) PESs. The prepared  $\text{Ar} \cdots \text{I}_2(\text{B}, \nu'=39, n'=0)$  level is close in energy with the *d* level in the  $\text{Ar} + \text{I}_2(\text{B}, \nu=38)$  PES that is localized in the T-shaped region of the intermolecular PES. It is quite possible that this level is not the only level involved in the IVR process, and this intermediate level can undergo IVR again, perhaps involving the *f* level in the  $\text{Ar} + \text{I}_2(\text{B}, \nu=37)$  PES. The last step in this dissociation pathway is VP from one of these intermediate levels to the continuum of states above the  $\text{Ar} + \text{I}_2(\text{B}, \nu=34)$  product channel. For the case where the accessible intermediate levels and the initially prepared level are localized in the T-shaped regions of the intermolecular PESs, dissociation would result in an  $\text{I}_2(\text{B}, \nu)$  VMI image with a negative anisotropy parameter. This would make  $\text{I}_2(\text{B}, \nu)$  fragments that dissociated from the intermediate doorway levels indistinguishable from fragments produced via direct VP into the  $\text{Ar} + \text{I}_2(\text{B}, \nu)$  dissociative continuum. For this reason, direct VP cannot be conclusively identified as the primary dissociation mechanism for these  $\nu'$  levels, even though the images have  $\beta < 0$ . Ultimately, the positive anisotropy parameters measured for the products of some of the  $\text{Ar} \cdots \text{I}_2(\text{B}, \nu', n'=0)$  levels included in **Table 1**, suggest that IVR-mediated VP does occur for those levels, and it could occur for the other levels.

We postulate that when multiple product channels are formed and the anisotropy of the  $\text{I}_2$  product VMI images associated with these channels have noticeably different anisotropy parameters, the  $\text{Ar} + \text{I}_2(\text{B}, \nu)$  products are formed from different pathways via IVR. **Table 1** lists a few  $\text{Ar} \cdots \text{I}_2(\text{B}, \nu', n'=0)$  levels for which the different  $\Delta\nu$  products have contrasting anisotropy parameters. For the case of  $\text{Ar} \cdots \text{I}_2(\text{B}, \nu'=39, n'=0)$ , dissociation via the  $\Delta\nu = -5$ ,  $-6$ , and  $-7$  channels, the  $\text{I}_2(\text{B}, \nu)$  product images have anisotropy parameters of  $-0.58(1)$ ,  $-0.33(1)$ , and  $-0.02(2)$ , respectively. As mentioned, the  $\text{Ar} \cdots \text{I}_2(\text{B}, \nu'=39, n'=0)$  level is close in energy to levels *d* and *f* in the  $\text{Ar} + \text{I}_2(\text{B}, \nu=38)$  and  $\text{Ar} + \text{I}_2(\text{B}, \nu=37)$  PESs, respectively, and these have T-shaped geometries. The  $\text{Ar} \cdots \text{I}_2(\text{B}, \nu'=39, n'=0)$  level is also close in energy and could couple to the *g* and *o* delocalized levels bound within the  $\text{Ar} + \text{I}_2(\text{B}, \nu=36)$  and  $\text{Ar} + \text{I}_2(\text{B}, \nu=35)$  PESs, respectively. All of these dark levels, *d*, *f*, *g*, and *o*, can then couple to different  $\text{Ar} + \text{I}_2(\text{B}, \nu)$  dissociative continua, resulting in contributions from  $\text{I}_2(\text{B}, \nu)$  products with different anisotropy parameters.

There is a trend of the anisotropy parameter approaching zero with increasing kinetic energy release and larger change in  $\nu$  for the dissociation products of the  $\text{Ar} \cdots \text{I}_2(\text{B}, \nu'=39, n'=0)$  level. This is not the norm, however, for the levels investigated. The  $\text{I}_2(\text{B}, \nu)$  product images recorded for dissociation of the  $\text{Ar} \cdots \text{I}_2(\text{B}, \nu'=38, n'=0)$  level into the  $\Delta\nu = -4$ ,  $-5$ ,  $-6$ , and  $-7$  channels have anisotropy parameters that tend to increase,

$\beta = -0.25(2)$ ,  $-0.67(1)$ ,  $-0.80(2)$ , and  $-0.80(2)$ , respectively. As both the  $\text{Ar} + \text{I}_2(\text{B}, v'=39)$  and  $\text{Ar} + \text{I}_2(\text{B}, v'=38)$  PESs are nested within multiple PESs, IVR can occur with levels in any of these wells if there is sufficient energetic and wavefunction overlap between the initial bright and intermediate dark levels. The varying anisotropy parameters for each of the  $\text{I}_2(\text{B}, v)$  product images and different  $\Delta v$  product channels support the possibility that even for those levels and product channels with negative anisotropy parameters, IVR could be involved.

**Table 1** also lists a few  $\text{Ar}\cdots\text{I}_2(\text{B}, v', n'=0)$  levels for which  $v' > 16$ , yet the  $\Delta v$  product channels give  $\text{I}_2(\text{B}, v)$  fragments with isotropic angular distributions,  $\beta \sim 0$ . If IVR via levels in the lower  $\text{Ar} + \text{I}_2(\text{B}, v < v')$  PESs is occurring, there are several factors that can lead to isotropic angular distributions, even for T-shaped  $\text{Ar}\cdots\text{I}_2(\text{B}, v', n'=0)$  levels that dissociate promptly. As mentioned, those levels indicated by the red lines in **Fig. 5** have delocalized wavefunctions that sample linear geometries. With increasing intermolecular vibrational excitation, the position of the Ar atom about the  $\text{I}_2$  molecule becomes more delocalized and the wavefunctions can be described as hindered- or free-rotor states. If, prior to undergoing VP, the initial T-shaped level couples via IVR to any of these highly delocalized levels in which the Ar atom has amplitude over a wide range of angles, dissociation would occur from a broad range of angles, and the  $\text{I}_2(\text{B}, v)$  product images would be highly isotropic with  $\beta \approx 0$ .

$\text{I}_2(\text{B}, v)$  images with isotropic angular distributions could also result from parallel IVR pathways that sample multiple intermolecular vibrational levels in the  $\text{Ar} + \text{I}_2(\text{B}, v < v')$  PESs and form the same  $\text{Ar} + \text{I}_2(\text{B}, v)$  products. Consider the extreme case where one IVR pathway forms an  $\text{I}_2(\text{B}, v)$  product image with  $\beta = +2$ , or a  $\cos^2\theta$  distribution, and a second pathway results in an image with  $\beta = -1$ , or a  $\sin^2\theta$  distribution for that same product. The resultant image in this case would be a sum of the two product images, which would be isotropic, or  $\beta = 0$ , if the contributions from the two pathways are the same.

The anisotropy parameters of the  $\text{I}_2(\text{B}, v)$  product images measured when exciting the T-shaped,  $n'=0$  level in the PESs with  $v' = 27$  and  $37$  are approximately zero, and these may be examples of the prepared level undergoing parallel, competing dissociation pathways to the same product channel. The product image of the  $\Delta v = -4$  channel for the dissociation of the  $\text{Ar}\cdots\text{I}_2(\text{B}, v'=27, n'=0)$  level was determined to have  $\beta = -0.03(5)$ . Based on the spectral assignments of the intermolecular vibrational levels in the B-state PESs,<sup>61</sup> the  $\text{Ar}\cdots\text{I}_2(\text{B}, v'=27, n'=0)$  level is nearly resonant with at least two levels in different  $\text{Ar} + \text{I}_2(\text{B}, v < v')$  PESs; one level is localized in the T-shaped well in the  $\text{Ar} + \text{I}_2(\text{B}, v=26)$  PES, and the other is a delocalized level in the next lower  $\text{Ar} + \text{I}_2(\text{B}, v=25)$  PES. Similarly, the product image of the  $\Delta v = -5$  channel for the  $\text{Ar}\cdots\text{I}_2(\text{B}, v'=37, n'=0)$  level has a slightly positive anisotropy parameter,  $\beta = +0.07(1)$ . This bright level may be resonant with one dark T-shaped level in the  $\text{Ar} + \text{I}_2(\text{B}, v=36)$  PES and one delocalized level in the  $\text{Ar} + \text{I}_2(\text{B}, v=34)$  PES.

The significant density of states within each  $\text{Ar} + \text{I}_2(\text{B}, v')$  PES, especially near the dissociation limit, and the nesting of numerous PESs nested within each other suggest multiple dark levels may be sampled during dissociation, even when the

product image does not have an isotropic angular distribution. As already mentioned, the  $\text{I}_2(\text{B}, v, j)$  rotational distributions can provide information about the nature of the dark intermediate level sampled during dissociation.<sup>7,34,44-46</sup> Additional VMI experiments were performed to explore whether the product images measured as a function of  $\text{I}_2(\text{B}, v, j)$  product rotational excitation would reveal possible contributions from the dark levels accessed during the dissociation of the T-shaped  $\text{Ar}\cdots\text{I}_2(\text{B}, v', n'=0)$  levels.

Ion-yield spectra recorded with excitation of the T-shaped  $\text{Ar}\cdots\text{I}_2(\text{B}, v'=29, n'=0)$  level and probing the  $\Delta v = -5$  and  $-4$   $\text{I}_2(\text{B}, v)$  products are included in **Figs. 6(a)** and **(b)**. These spectra were collected using  $E_1 = 18462.27 \text{ cm}^{-1}$  and scanning  $E_2$  through the  $\text{I}_2$  E-B, 70-24 and 59-25 spectral regions, respectively. Ion counts from the background linear signals were subtracted from the ion-yield spectra so that only contributions from excitation of the T-shaped  $\text{Ar}\cdots\text{I}_2(\text{B}, v'=29, n'=0)$  level were obtained. These ion-yield spectra reveal the rotational state distributions for these product channels. Both spectra include a

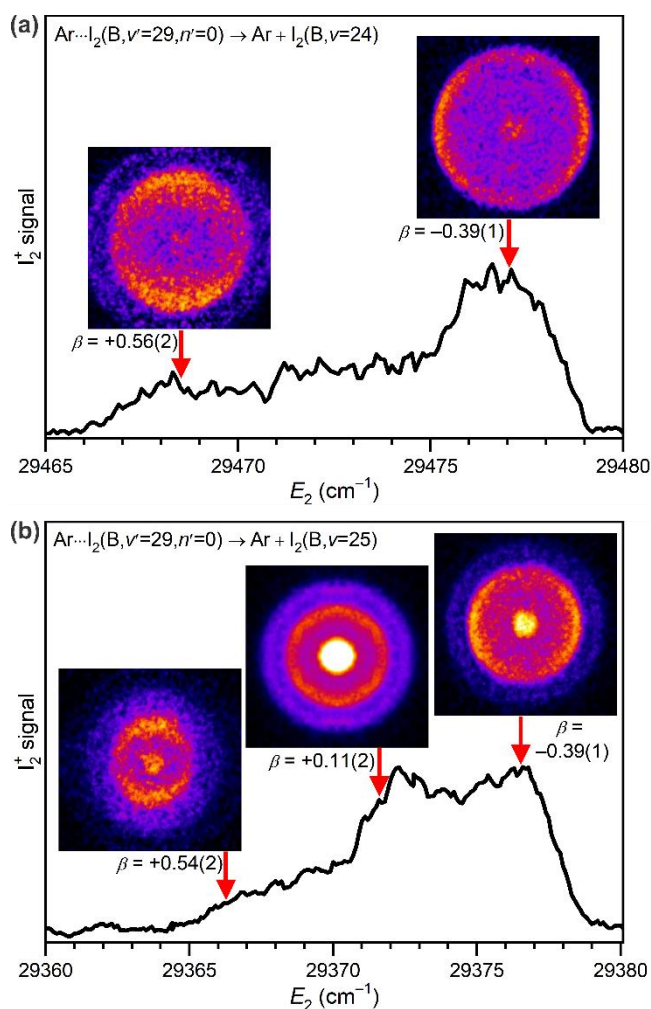


**Fig. 6** Ion-yield spectra for dissociation of T-shaped  $\text{Ar}\cdots\text{I}_2(\text{B}, v'=29, n'=0)$  to **(a)**  $\text{Ar} + \text{I}_2(\text{B}, v=24)$  and **(b)**  $\text{Ar} + \text{I}_2(\text{B}, v=25)$  fragments. The spectra have been corrected for linear, background signals. For clarity, the lower (higher) rotational states contribute to the higher (lower) energy regions of the spectrum. The arrows indicate the probe transitions used to collect the included  $\text{I}_2^+$  images.

tail extending to lower energies or to high  $I_2(B,v,j)$  product rotational states. Using known rotational constants for the  $I_2(E)$  and  $I_2(B)$  states,<sup>63</sup> the rotational distribution was simulated. The  $I_2(B,v,j)$  fragments from both the  $\Delta v = -5$  and  $\Delta v = -4$  product channels have rotational excitation up to  $j \sim 14$ .

Multiple  $I_2(B,v,j)$  product images were recorded with  $E_2$  fixed at varying energies within the breadth of the ion-yield spectra, indicated with arrows in **Fig. 6**. Probing the cold (low  $j$ ) fragments at higher  $E_2$  resulted in ion images with negative anisotropy parameters. In contrast, the product images obtained when probing the rotationally excited fragments have positive anisotropy parameters, which suggest dissociation from a linear geometry. These results indicate the  $Ar \cdots I_2(B,v',n'=0)$  level dissociates into a given  $\Delta v$   $Ar + I_2(B,v)$  product channel via different competing pathways, and these different pathways yield products with contrasting amounts of rotational excitation.

## Conclusions

In this perspective, we provided a brief overview of different types of dissociation mechanisms that can occur within weakly-bound, photoexcited rare gas-dihalogen van der Waals complexes,  $Rg \cdots X_2$ . Particular attention was given to direct VP and IVR mechanisms since their contributions can be challenging to untangle. The results of many previous experiments suggested preferences of VP over IVR for certain  $Rg \cdots X_2$  complexes and dihalogen vibrational excitation, and vice versa. Theory has supported many of these conclusions. The dynamics and product channels formed depend in complicated ways on the relative energetics of the dissociation channels, the binding energy of the complex, and the densities of states that may couple with the initially prepared intermolecular vibrational level.

In order to help shed light on the competition between VP and IVR, we presented results on the  $Ar \cdots I_2$  complex obtained using VMI experiments. Many of the  $I_2(B,v)$  product angular distributions measured following photoexcitation to a T-shaped  $Ar \cdots I_2(B,v',n'=0)$  level reveal the geometry of the complex sampled in the final step of the dissociation. The angular anisotropies of the  $I_2(B,v)$  product images indicate dissociation does not always occur from a rigid T-shaped geometry. Instead, dissociation sometimes occurs from a preferential linear intermolecular geometry. The change in geometry that occurs between photoexcitation and dissociation is associated with IVR and the nature of the excited intermolecular levels in the lower  $Ar + I_2(B,v)$  PESs that are accessed. The energetic overlap of the initially prepared  $Ar \cdots I_2(B,v',n'=0)$  level and the excited  $Ar \cdots I_2(B,v < v', n' > 0)$  intermolecular levels were estimated using spectroscopic assignments of the complexes in the  $I_2 B-X$ ,  $v'-0$  region<sup>61</sup> to propose the  $Ar \cdots I_2(B,v)$  levels that may be participating in the IVR. The anisotropies of the  $I_2(B,v)$  product images were found to vary strongly with the  $I_2$  vibrational excitation of the  $Ar \cdots I_2(B,v',n'=0)$  level initially prepared and on the  $\Delta v$  product channel. These results indicate that IVR occurs in the sparse density regime for  $Ar \cdots I_2$ , and the  $Ar + I_2(B,v)$  products are formed via different dissociation pathways. Furthermore, even within a single  $Ar + I_2(B,v)$  product channel,

the angular anisotropy of the product images depend on the rotational excitation of the product. In summary, the results of these VMI experiments demonstrate that complexes prepared in many of the T-shaped  $Ar \cdots I_2(B,v',n'=0)$  levels undergo IVR-mediated VP and not direct VP from the initially prepared level.

In terms of broader impacts beyond the investigation of the dynamics in  $Rg \cdots X_2$  complexes, these experiments further illustrate the utility of combining vibronic laser spectroscopy with VMI for disentangling complicated and competing reaction dynamics. In addition to directly probing the angular distributions of specific vibrational product channels, it can also be informative to do experiments as a function of rotational excitation of the products. It would be straightforward to expand these types of measurements to probing the photodissociation of other weakly-bound complexes or even large molecules with internal degrees of freedom.

## Conflicts of interest

There are no conflicts to declare.

## Acknowledgements

This work was partially supported by the NSF under grant CSDMA-2102241. Acknowledgment is made to the donors of the American Chemical Society Petroleum Research Fund for partial support of this research.

## References

- 1 J. E. Kenny, K. E. Johnson, W. Sharfin and D. H. Levy, *J. Chem. Phys.*, 1980, **72**, 1109-1119.
- 2 K. E. Johnson, W. Sharfin and D. H. Levy, *J. Chem. Phys.*, 1981, **74**, 163-170.
- 3 J. A. Beswick and J. Jortner, *Advan. Chem. Phys.*, 1981, **47**, 363.
- 4 N. Goldstein, T. L. Brack and G. H. Atkinson, *J. Chem. Phys.*, 1986, **85**, 2684-2691.
- 5 E. R. Bernstein, *Ann. Rev. Phys. Chem.*, 1995, **46**, 197.
- 6 M. I. Lester, *Advan. Chem. Phys.*, 1996, **96**, 51-102.
- 7 A. Rohrbacher, N. Halberstadt and K. C. Janda, *Ann. Rev. Phys. Chem.*, 2000, **51**, 405-433.
- 8 A. Rohrbacher, J. Williams and K. C. Janda, *Phys. Chem. Chem. Phys.*, 1999, **1**, 5263-5276.
- 9 A. Buchachenko, N. Halberstadt, B. Lepetit and O. Roncero, *Int. Rev. Phys. Chem.*, 2003, **22**, 153-202.
- 10 J. A. Beswick, N. Halberstadt and K. C. Janda, *Chem. Phys.*, 2012, **399**, 4-16.
- 11 R. L. Waterland, J. M. Skene and M. I. Lester, *J. Chem. Phys.*, 1988, **89**, 7277-7286.
- 12 A. B. McCoy, J. P. Darr, D. S. Boucher, P. R. Winter, M. D. Bradke and R. A. Loomis, *J. Chem. Phys.*, 2004, **120**, 2677-2685.
- 13 D. B. Strasfeld, J. P. Darr and R. A. Loomis, *Chem. Phys. Lett.*, 2004, **397**, 116-122.

- 14 N. Zeigler, C. Makarem, J. Wei and R. A. Loomis, *J. Chem. Phys.*, 2020, **152**, 094303.
- 15 M. S. Kim, R. E. Smalley, L. Wharton and D. H. Levy, *J. Chem. Phys.*, 1976, **65**, 1216-1217.
- 16 R. E. Smalley, D. H. Levy and L. Wharton, *J. Chem. Phys.*, 1976, **64**, 3266-3276.
- 17 W. Sharfin, K. E. Johnson, L. Wharton and D. H. Levy, *J. Chem. Phys.*, 1979, **71**, 1292-1299.
- 18 J. A. Blazy, B. M. DeKoven, T. D. Russell and D. H. Levy, *J. Chem. Phys.*, 1980, **72**, 2439-2444.
- 19 G. Delgado-Barrio, P. Villarreal, P. Mareca and G. Albelda, *J. Chem. Phys.*, 1983, **78**, 280-284.
- 20 J. M. Skene and M. I. Lester, *Chem. Phys. Lett.*, 1985, **116**, 93-99.
- 21 J. M. Skene, J. C. Drobits and M. I. Lester, *J. Chem. Phys.*, 1986, **85**, 2329-2331.
- 22 J. I. Cline, D. D. Evard, B. P. Reid, N. Sivakumar, F. Thommen and K. C. Janda, in *Structure and dynamics of weakly bound molecular complexes*, ed. A. Weber, D. Reidel Publishing Company, Dordrecht, Holland 1987, pp. 533-551.
- 23 J. I. Cline, N. Sivakumar, D. D. Evard and K. C. Janda, *J. Chem. Phys.*, 1987, **86**, 1636-1637.
- 24 N. Halberstadt, J. A. Beswick and K. C. Janda, *J. Chem. Phys.*, 1987, **87**, 3966-3975.
- 25 J. I. Cline, B. P. Reid, D. D. Evard, N. Sivakumar, N. Halberstadt and K. C. Janda, *J. Chem. Phys.*, 1988, **89**, 3535-3552.
- 26 D. D. Evard, C. R. Bieler, J. I. Cline, N. Sivakumar and K. C. Janda, *J. Chem. Phys.*, 1988, **89**, 2829-2838.
- 27 J. I. Cline, N. Sivakumar, D. D. Evard, C. R. Bieler, B. P. Reid, N. Halberstadt, S. R. Hair and K. C. Janda, *J. Chem. Phys.*, 1989, **90**, 2605-2616.
- 28 R. L. Waterland, M. I. Lester and N. Halberstadt, *J. Chem. Phys.*, 1990, **92**, 4261-4271.
- 29 M. L. Burke and W. Klemperer, *J. Chem. Phys.*, 1993, **98**, 6642-6650.
- 30 D. G. Jahn, S. G. Clement and K. C. Janda, *J. Chem. Phys.*, 1994, **101**, 283-291.
- 31 A. Rohrbacher, T. Ruchti, K. C. Janda, A. A. Buchachenko, M. I. Hernández, T. González-Lezana, P. Villarreal and G. Delgado-Barrio, *J. Chem. Phys.*, 1999, **110**, 256-266.
- 32 A. Burroughs, G. Kerenskaya and M. C. Heaven, *J. Chem. Phys.*, 2001, **115**, 784-791.
- 33 A. García-Vela and K. C. Janda, *J. Chem. Phys.*, 2006, **124**, 034305.
- 34 B. Kubiak, P. S. H. Fitch, L. Wharton and D. H. Levy, *J. Chem. Phys.*, 1978, **68**, 4477-4480.
- 35 N. Halberstadt, S. Serna, A. Roncero and K. C. Janda, *J. Chem. Phys.*, 1992, **97**, 341-354.
- 36 N. Halberstadt, J. A. Beswick, O. Roncero and K. C. Janda, *J. Chem. Phys.*, 1992, **96**, 2404-2407.
- 37 O. Roncero, P. Villarreal, G. Delgado-Barrio, N. Halberstadt and K. C. Janda, *J. Chem. Phys.*, 1993, **99**, 1035-1049.
- 38 S. K. Gray and O. Roncero, *J. Phys. Chem.*, 1995, **99**, 2512-2519.
- 39 O. Roncero and S. K. Gray, *J. Chem. Phys.*, 1996, **104**, 4999-5011.
- 40 K. C. Janda, O. Roncero and N. Halberstadt, *J. Chem. Phys.*, 1996, **105**, 5830-5841.
- 41 O. Roncero, D. Caloto, K. C. Janda and N. Halberstadt, *J. Chem. Phys.*, 1997, **107**, 1406-1419.
- 42 E. M. Goldfield and S. K. Gray, *Chem. Phys. Lett.*, 1997, **276**, 1-8.
- 43 T. Gonzalez-Lezana, M. I. Hernandez, G. Delgado-Barrio and P. Villarreal, *J. Chem. Phys.*, 1997, **106**, 3216-3226.
- 44 C. F. Kunz, I. Burghardt and B. A. Heß, *J. Chem. Phys.*, 1998, **109**, 359-366.
- 45 A. E. Stevens Miller, C.-C. Chuang, H. C. Fu, K. J. Higgins and W. Klemperer, *J. Chem. Phys.*, 1999, **111**, 7844-7856.
- 46 A. Burroughs and M. C. Heaven, *J. Chem. Phys.*, 2001, **114**, 7027-7035.
- 47 O. Roncero, A. A. Buchachenko and B. Lepetit, *J. Chem. Phys.*, 2005, **122**, 034303.
- 48 A. Garcia-Vela, *J. Chem. Phys.*, 2007, **126**, 124306.
- 49 J. Cabrera, C. R. Bieler, N. McKinney, W. E. van der Veer, J. M. Pio, K. Janda and O. Roncero, *J. Chem. Phys.*, 2007, **127**, 164309.
- 50 J. P. Darr, R. A. Loomis and A. B. McCoy, *J. Chem. Phys.*, 2005, **122**, 044318.
- 51 M. Bixon and J. Jortner, *J. Chem. Phys.*, 1969, **50**, 3284-3290.
- 52 F. Lahmani, A. Tramer and C. Tric, *J. Chem. Phys.*, 1974, **60**, 4431-4447.
- 53 B. Lepetit, O. Roncero, A. A. Buchachenko and N. Halberstadt, *J. Chem. Phys.*, 2002, **116**, 8367-8375.
- 54 M. A. Taylor, J. M. Pio, W. E. van der Veer and K. C. Janda, *J. Chem. Phys.*, 2010, **132**, 104309.
- 55 K. E. Johnson, L. Wharton and D. H. Levy, *J. Chem. Phys.*, 1978, **69**, 2719-2724.
- 56 L. J. van de Burgt, J.-P. Nicolai and M. C. Heaven, *J. Chem. Phys.*, 1984, **81**, 5514-5520.
- 57 D. G. Jahn, W. S. Barney, J. Cabalo, S. G. Clement, A. Rohrbacher, T. J. Slotterback, J. Williams and K. C. Janda, *J. Chem. Phys.*, 1996, **104**, 3501-3510.
- 58 D. D. Evard, J. I. Cline and K. C. Janda, *J. Chem. Phys.*, 1988, **88**, 5433-5438.
- 59 J. A. Cabrera, C. R. Bieler, B. C. Olbricht, W. E. van der Veer and K. C. Janda, *J. Chem. Phys.*, 2005, **123**, 054311.
- 60 J. Wei, C. Makarem, A. L. Reinitz, J. P. Darr and R. A. Loomis, *Chem. Phys.*, 2012, **399**, 172-179.
- 61 C. Makarem and R. A. Loomis, *Chem. Phys. Lett.*, 2016, **651**, 119-123.
- 62 O. Roncero, B. Lepetit, J. A. Beswick, N. Halberstadt and A. A. Buchachenko, *J. Chem. Phys.*, 2001, **115**, 6961-6973.
- 63 J. C. D. Brand, A. R. Hoy, A. K. Kalkar and A. B. Yamashita, *J. Mol. Spect.*, 1982, **95**, 350-358.
- 64 A. T. J. B. Eppink and D. H. Parker, *Rev. Sci. Instrum.*, 1997, **68**, 3477-3484.
- 65 V. Dribinski, A. Ossadtchi, V. A. Mandelshtam and H. Reisler, *Rev. Sci. Instrum.*, 2002, **73**, 2634-2642.
- 66 R. N. Zare, *Mol. Photochem.*, 1972, **4**, 1-37.